November 1996

Photoionization of Atoms

Anthony F. Starace
University of Nebraska-Lincoln, astarace1@unl.edu

24

Photoionization of Atoms

Anthony F. Starace

Department of Physics and Astronomy, The University of Nebraska, Lincoln, Nebraska 68588-0111

24.1 INTRODUCTION

This chapter outlines the theory of atomic photoionization, and the dynamics of the photon-atom collision process. Those kinds of electron correlation that are most important in photoionization are emphasized, although many qualitative features can be understood within a central field model. The particle-hole type of electron correlations are discussed, as they are by far the most important for describing the single photoionization of atoms near ionization thresholds. Detailed reviews of atomic photoionization are presented in Refs. [1] and [2]. Current activities and interests are well-described in two recent books [3, 4]. Other related topics covered in this volume are, experimental studies of photon interactions at both low and high energies in Chaps. 59 and 60, photodetachment in Chap. 58, and theoretical descriptions of electron correlations in Chap. 23, autoionization in Chap. 25, and multiphoton processes in Chap. 72.

24.2 GENERAL CONSIDERATIONS

24.2.1 The Interaction Hamiltonian

Consider an N-electron atom with nuclear charge Z. In nonrelativistic approximation, it is described by the Hamiltonian

$$H = \sum_{i=1}^{N} \left(\frac{{p_i}^2}{2m} - \frac{Ze^2}{r_i} \right) + \sum_{i>j=1}^{N} \frac{e^2}{|\mathbf{r}_i - \mathbf{r}_j|} . \qquad (24.1)$$

The one-electron terms in brackets describe the kinetic and potential energy of each electron in the Coulomb field of the nucleus; the second set of terms describe the repulsive electrostatic potential energy between electron pairs. The interaction of this atom with external electromagnetic radiation is described by the additional terms obtained upon replacing $\mathbf{p}_i$ by $\mathbf{p}_i + (|e|/c)\mathbf{A}(\mathbf{r}_i, t)$, where $\mathbf{A}(\mathbf{r}_i, t)$ is the vector potential for the radiation. The interaction Hamiltonian is thus

$$H_{\text{int}} = \sum_{i=1}^{N} \left\{ \frac{+|e|}{2mc} [\mathbf{p}_i \cdot \mathbf{A}(\mathbf{r}_i, t) + \mathbf{A}(\mathbf{r}_i, t) \cdot \mathbf{p}_i] + \frac{e^2}{2mc^2} |\mathbf{A}(\mathbf{r}_i, t)|^2 \right\} . \qquad (24.2)$$

Under the most common circumstance of single-photon ionization of an outer-subshell electron, the interaction Hamiltonian in (24.2) may be simplified considerably. First, the third term in (24.2) may be dropped, as it introduces two-photon processes (since it is of second order in $\mathbf{A}$). In any case, it is small compared with single photon processes since it is of second order in the coupling constant $|e|/c$. Second, we choose the Coulomb gauge for $\mathbf{A}$, which fixes the divergence of $\mathbf{A}$ as $\nabla \cdot \mathbf{A} = 0$. $\mathbf{A}$ thus describes a transverse radiation field. Furthermore $\mathbf{p}$ and $\mathbf{A}$ now commute and hence the first and second terms in (24.2) may be combined. Third, we introduce the following form for $\mathbf{A}$:

$$\mathbf{A}(\mathbf{r}_i, t) = \left(\frac{2\pi c^2 \hbar}{\omega V} \right)^{\frac{1}{2}} \hat{\boldsymbol{\epsilon}} e^{i(\mathbf{k} \cdot \mathbf{r}_i - \omega t)} . \qquad (24.3)$$

This classical expression for $\mathbf{A}$ may be shown [5] to give photoabsorption transition rates that are in agreement with those obtained using the quantum theory of radiation. Here $\mathbf{k}$ and ω are the wave vector and angular frequency of the incident radiation, $\hat{\boldsymbol{\epsilon}}$ is its polarization unit vector, and V is the spatial volume. Fourth, the *electric dipole* (E1) approximation, in which $\exp i(\mathbf{k} \cdot \mathbf{r}_i)$ is replaced by unity, is usually appropriate. The radii r_i of the atomic electrons are usually of order 1Å. Thus for $\lambda \gg 100\text{Å}, |\mathbf{k} \cdot \mathbf{r}_i| \ll 1$. Now $\lambda \gg 100\text{Å}$ corresponds to photon energies $\hbar\omega \ll 124\text{eV}$. For outer atomic subshells, most of the photoabsorption occurs for much smaller photon energies, thus validating the use of the E1 approximation.[1] Use of all of the above conventions and approximations allows the reduction of H_{int} in Eq. (24.2) to the simplified form

$$H_{\text{int}} = \frac{+|e|}{mc} \left(\frac{2\pi c^2 \hbar}{\omega V} \right)^{\frac{1}{2}} \sum_{i=1}^{N} \hat{\boldsymbol{\epsilon}} \cdot \mathbf{p}_i \exp(-i\omega t) . \qquad (24.4)$$

H_{int} thus has the form of a harmonically time-dependent perturbation. According to time-dependent perturbation theory, the photoionization cross section is proportional to the absolute square of the matrix element of (24.4) between the initial and final electronic states described by the atomic Hamiltonian in (24.1). Atomic units, in which $|e| = m = \hbar = 1$, are used in what follows.

24.2.2 Alternative Forms for the Transition Matrix Element

The matrix element of (24.4) is proportional to the matrix element of the momentum operator $\sum_i \mathbf{p}_i$. Alternative expressions for this matrix element may be obtained from the following operator equations involving commutators of the exact atomic Hamiltonian in (24.1):

$$\sum_{i=1}^{N} \mathbf{p}_i = -i \left[\sum_{i=1}^{N} \mathbf{r}_i, H \right] , \qquad (24.5)$$

$$\left[\sum_{i=1}^{N} \mathbf{p}_i, H \right] = -i \sum_{i=1}^{N} \frac{Z\mathbf{r}_i}{r_i^3} . \qquad (24.6)$$

Matrix elements of (24.5) and (24.6) between eigenstates $\langle \psi_0 |$ and $|\psi_f\rangle$ of H having energies E_0 and E_f respectively give

$$\langle \psi_0 | \sum_{i=1}^{N} \mathbf{p}_i | \psi_f \rangle = -i\omega \langle \psi_0 | \sum_{i=1}^{N} \mathbf{r}_i | \psi_f \rangle , \qquad (24.7)$$

$$\langle \psi_0 | \sum_{i=1}^{N} \mathbf{p}_i | \psi_f \rangle = \frac{-i}{\omega} \langle \psi_0 | \sum_{i=1}^{N} \frac{Z\mathbf{r}_i}{r_i^3} | \psi_f \rangle , \qquad (24.8)$$

where $\omega = E_f - E_0$. Matrix elements of $\sum_{i=1}^{N} \mathbf{p}_i$, $\sum_{i=1}^{N} \mathbf{r}_i$, and $\sum_{i=1}^{N} Z\mathbf{r}_i/r_i^3$ are known as the "velocity," "length," and "acceleration" forms of the E1 matrix element.

Equality of the matrix elements in (24.7) and (24.8) does not hold when approximate eigenstates of H are used [6]. In such a case, qualitative considerations may help to determine which form is most reliable. For example, the length form tends to emphasize the large r part of the approximate wave functions, the acceleration form tends to emphasize the small r part of the wave functions, and the velocity form tends to emphasize intermediate values of r.

If instead of employing approximate eigenstates of the exact H, one employs exact eigenstates of an approximate N-electron Hamiltonian, then inequality of the matrix elements in (24.7) and (24.8) is a measure of the nonlocality of the potential in the approximate Hamiltonian

[1] This approximation cannot be used uncritically, however. For example, photoionization of excited atoms (which have large radii), photoionization of inner subshells (which requires the use of short wavelength radiation), and calculation of differential cross sections or other measurable quantities that are sensitive to the overlap of electric dipole and higher multipole amplitudes all require that the validity of the electric dipole approximation be checked.

[7]. The exchange part of the Hartree-Fock potential is an example of such a nonlocal potential. Nonlocal potentials are also implicitly introduced in configuration interaction calculations employing a finite number of configurations [7]. One may eliminate the ambiguity of which form of the E1 transition operator to use by requiring that the Schrödinger equation be gauge invariant. Only the length form is consistent with such gauge invariance [7].

However, equality of the alternative forms of the transition operator does not necessarily imply high accuracy. For example, they are exactly equal when one uses an approximate local potential to describe the N-electron atom, as in a central potential model, even though the accuracy is often poor. The length and velocity forms are also exactly equal in the random phase approximation [8], which does generally give accurate cross sections for single photoionization of closed shell atoms. No general prescription exists, however, for ensuring that the length and velocity matrix elements are equal at each level of approximation to the N-electron Hamiltonian.

24.2.3 Selection Rules for Electric Dipole Transitions

If one ignores relativistic interactions, then a general atomic photoionization process may be described in LS-coupling as follows:

$$\begin{aligned}&\mathcal{A}(L,S,M_L,M_S,\pi_{\mathcal{A}})+\gamma(\pi_\gamma,\ell_\gamma,m_\gamma)\\&\longrightarrow \mathcal{A}^+(\bar{L}\bar{S}\pi_{\mathcal{A}^+})\varepsilon\ell(L',S',M_{L'},M_{S'})\,.\end{aligned}\tag{24.9}$$

Here the atom $\mathcal{A}$ is ionized by the photon γ to produce a photoelectron with kinetic energy ε and orbital angular momentum ℓ. The photoelectron is coupled to the ion $\mathcal{A}^+$ with total orbital and spin angular momenta L' and S'. In the electric dipole approximation, the photon may be regarded as having odd parity, i.e., $\pi_\gamma = -1$, and unit angular momentum, i.e., $\ell_\gamma = 1$. This is obvious from Eqs. (24.7) and (24.8), where the E1 operator is seen to be a vector operator. The component m_γ of the photon in the E1 approximation is ± 1 for right or left circularly polarized light and 0 for linearly polarized light.[2] Angular momentum and parity selection rules for the E1 transition in (24.9) imply the following relations between the initial and final state quantum numbers:

$$L' = L \oplus 1 = \bar{L} \oplus \ell\,, \tag{24.10}$$

$$M_{L'} = M_L + m_\gamma = M_{\bar{L}} + m_\ell\,, \tag{24.11}$$

$$S' = S = \bar{S} \oplus \tfrac{1}{2}\,, \tag{24.12}$$

$$M_{S'} = M_S = M_{\bar{S}} + m_s\,, \tag{24.13}$$

$$\pi_{\mathcal{A}}\pi_{\mathcal{A}^+} = (-1)^{\ell+1}\,. \tag{24.14}$$

[2]The z axis is taken as $\hat{\mathbf{k}}$ in the case of circularly polarized light and as $\hat{\boldsymbol{\epsilon}}$ in the case of linearly polarized light, where $\mathbf{k}$ and $\hat{\boldsymbol{\epsilon}}$ are defined in Eq. (24.3).

Equation (24.14) follows from the parity $(-1)^\ell$ of the photoelectron. The direct sum symbol $\oplus$ denotes the vector addition of $\mathbf{A}$ and $\mathbf{B}$ i.e, $\mathbf{A} \oplus \mathbf{B} = A+B, A+B-1, \ldots, |A-B|$.

In (24.9), the quantum numbers $\alpha \equiv \bar{L}, \bar{S}, \pi_{\mathcal{A}^+}, \ell, L', S', M_{L'}, M_{S'}$ (plus any other quantum numbers needed to specify uniquely the state of the ion $\mathcal{A}^+$) define a final state *channel.* All final states that differ only in the photoelectron energy ε belong to the same channel. The quantum numbers $L', S', M_{L'}, M_{S'}$, and $\pi_{\rm tot} = (-1)^\ell \pi_{\mathcal{A}^+}$ are the only good quantum numbers for the final states. Thus the Hamiltonian (24.1) mixes final state channels having the same angular momentum and parity quantum numbers but differing quantum numbers for the ion and the photoelectron; i.e., differing $\bar{L}, \bar{S}$, π_{A^+}, and ℓ but the same $L', S', M_{L'}, M_{S'}$ and $(-1)^\ell \pi_{\mathcal{A}^+}$.

24.2.4 Boundary Conditions on the Final State Wave Function

Photoionization calculations obtain final state wave functions statisfying the asymptotic boundary condition that the photoelectron is ionized in channel α. This boundary condition is expressed as

$$\begin{aligned}&\psi^-_{\alpha E}(\mathbf{r}_1\mathbf{s}_1,\ldots,\mathbf{r}_N\mathbf{s}_N)\\&\quad\underset{r_N\to\infty}{\longrightarrow}\theta_\alpha(\mathbf{r}_1 s_1,\ldots,\hat{\mathbf{r}}_N\mathbf{s}_N)\frac{1}{i(2\pi k_\alpha)^{\frac{1}{2}}}\frac{1}{r_N}e^{i\Delta_\alpha}\\&\qquad-\sum_{\alpha'}\theta_{\alpha'}(\mathbf{r}_1\mathbf{s}_1,\ldots,\hat{\mathbf{r}}_N\mathbf{s}_N)\frac{1}{i(2\pi k_{\alpha'})^{\frac{1}{2}}}\frac{1}{r_N}e^{-i\Delta_{\alpha'}}S^\dagger_{\alpha'\alpha}\,,\end{aligned}\tag{24.15}$$

where the phase appropriate for a Coulomb field is

$$\Delta_\alpha \equiv k_\alpha r_N - \tfrac{1}{2}\pi\ell_\alpha + \frac{1}{k_\alpha}\log 2k_\alpha r_N + \sigma_{\ell_\alpha}\,. \tag{24.16}$$

The minus superscript on the wave function in (24.15) indicates an "incoming wave" normalization: i.e., asymptotically $\psi^-_{\alpha E}$ has outgoing spherical Coulomb waves only in channel α, while there are incoming spherical Coulomb waves in all channels. $S^\dagger_{\alpha'\alpha}$ is the Hermitian conjugate of the S-matrix of scattering theory, θ_α indicates the coupled wave function of the ion and the angular and spin parts of the photoelectron wave function, k_α is the photoelectron momentum in channel α and ℓ_α is its orbital angular momentum, and σ_{ℓ_α} in (24.16) is the Coulomb phase shift.

While one calculates channel functions $\psi^-_{\alpha E}$, experimentally one measures photoelectrons which asymptotically have well-defined linear momenta $\mathbf{k}_\alpha$ and well-defined spin states $m_{\frac{1}{2}}$, and ions in well-defined states $\bar{\alpha} \equiv \bar{L}\bar{S}M_{\bar{L}}M_{\bar{S}}$. The wave function appropriate for this experimental situation is related to the channel functions by uncoupling the ionic and electronic orbital and spin

angular momenta and projecting the photoelectron angular momentum states ℓ_α, m_α onto the direction $\hat{\mathbf{k}}_\alpha$ by means of the spherical harmonic $Y^\star_{\ell_\alpha m_\alpha}(k_\alpha)$. This relation is [1]:

$$\psi^-_{\bar{\alpha}k_\alpha}(\mathbf{r}_1\mathbf{s}_1,\ldots,\mathbf{r}_N\mathbf{s}_N) = \sum_{\ell_\alpha m_\alpha} \frac{i^{\ell_\alpha}\exp(-i\sigma_{\ell_\alpha})}{k_\alpha^{\frac{1}{2}}} Y^\star_{\ell_\alpha m_\alpha}(\hat{\mathbf{k}}_\alpha) \sum_{LM_LSM_S} \langle \bar{L}M_{\bar{L}}\ell_\alpha m_\alpha | LM_L\rangle \times \langle \bar{S}M_{\bar{S}}\tfrac{1}{2}m_{\frac{1}{2}} | SM_S\rangle \psi^-_{\alpha E}(\mathbf{r}_1\mathbf{s}_1,\ldots,\mathbf{r}_N\mathbf{s}_N)\,, \quad (24.17)$$

where the coefficients in brackets are Clebsch-Gordan coefficients. This wave function is normalized to a delta function in momentum space, i.e.,

$$\int (\psi^-_{\bar{\alpha}\mathbf{k}_\alpha})^\dagger \psi^-_{\bar{\alpha}'\mathbf{k}_{\alpha'}} d^3\mathbf{r} = \delta_{\bar{\alpha}\bar{\alpha}'}\delta(\mathbf{k}_\alpha - \mathbf{k}_{\alpha'})\,. \quad (24.18)$$

The factors $i^{\ell_\alpha}\exp(-i\sigma_{\ell_\alpha})k_\alpha^{-\frac{1}{2}}$ ensure that for large r_N Eq. (24.17) represents a Coulomb wave (with momentum $\mathbf{k}_\alpha$) times the ionic wave function for the state $\bar{\alpha}$ plus a sum of terms representing incoming spherical waves. Thus only the ionic term $\bar{\alpha}$ has an outgoing wave. One uses the wave function in (24.17) to calculate the angular distribution of photoelectrons.

24.2.5 Photoionization Cross Sections

If one writes $H_{\rm int}$ in (24.4) as $H_{\rm int}(t) = H_{\rm int}(0)^{-i\omega t}$, then from first order time-dependent perturbation theory, the transition rate for transition from an initial state with energy E_0 and wave function ψ_0 to a final state with total energy E_f and wave function $\psi^-_{\bar{\alpha}\mathbf{k}_\alpha}$ is

$$dW_{\mathbf{k}_\alpha} = 2\pi|\langle\psi_0|H_{\rm int}(0)|\psi^-_{\bar{\alpha}\mathbf{k}_\alpha}\rangle|^2 \times \delta(E_f - E_0 - \omega)k_\alpha^2 dk_\alpha d\Omega(\hat{\mathbf{k}}_\alpha)\,. \quad (24.19)$$

The delta function expresses energy conservation and the last factors on the right are the phase space factors for the photoelectron. Dividing the transition rate by the incident photon current density c/V, integrating over dk_α, and inserting $H_{\rm int}(0)$, the differential photoionization cross section is

$$\frac{d\sigma_{\bar{\alpha}}}{d\Omega} = \frac{4\pi^2}{c}\frac{k_\alpha}{\omega}\,|\hat{\boldsymbol{\epsilon}}\cdot\langle\psi_0|\sum_{i=1}^N \mathbf{p}_i|\psi^-_{\bar{\alpha}\mathbf{k}_\alpha}\rangle|^2\,. \quad (24.20)$$

Implicit in Eqs. (24.19) and (24.20) is an average over initial magnetic quantum numbers $M_{L_0}M_{S_0}$ and a sum over final magnetic quantum numbers $M_{\bar{L}}M_{\bar{S}}m_{\frac{1}{2}}$. The length form of Eq. (24.20) is obtained by replacing each $\mathbf{p}_i$ by $\omega\mathbf{r}_i$ [*cf.* Eq. (24.7)].

Substitution of the final state wave function (24.17) in Eq. (24.20) permits one to carry out the numerous summations over magnetic quantum numbers and obtain the form

$$\frac{d\sigma_{\bar{\alpha}}}{d\Omega} = \frac{\sigma_{\bar{\alpha}}}{4\pi}\left[1 + \beta P_2(\cos\theta)\right] \quad (24.21)$$

for the differential cross section [9]. Here $\sigma_{\bar{\alpha}}$ is the partial cross section for leaving the ion in the state $\bar{\alpha}$, β is the asymmetry parameter [10], $P_2(\cos\theta) = \frac{3}{2}\cos^2\theta - \frac{1}{2}$, and θ indicates the direction of the outgoing photoelectron with respect to the polarization vector $\hat{\boldsymbol{\epsilon}}$ of the incident light. The form of (24.21) follows in the electric dipole aproximation from general symmetry principles, provided that the target atom is unpolarized [11]. The partial cross section is given in terms of reduced E1 matrix elements involving the channel functions in (24.15) by

$$\sigma_{\bar{\alpha}} = \frac{4\pi^2}{3c}\,\omega[L]^{-1}\sum_{\ell_\alpha L'}|\langle\psi_0\parallel\sum_{i=1}^N r_i{}^{[1]}\parallel\psi^-_{\alpha E}\rangle|^2\,. \quad (24.22)$$

The β parameter has a much more complicated expression involving interference between different reduced dipole amplitudes [10]. Thus measurement of β provides information on the relative phases of the alternative final state channel wave functions, whereas the partial cross-section in Eq. (24.22) does not. From the requirement that the differential cross section in (24.21) be positive, one sees that $-1 \le \beta \le +2$.

24.3 AN INDEPENDENT ELECTRON MODEL

The many-body wave functions ψ_0 and $\psi^-_{\alpha E}$ are usually expressed in terms of a basis of independent electron wave functions. Key qualitative features of photoionization cross sections can often be interpreted in terms of the overlaps of initial and final state one electron radial wave functions [12]. The simplest independent electron representation of the atom, the central potential model, proves useful for this purpose.

24.3.1 Central Potential Model

In the central potential (CP) model the exact H in (24.1) is approximated by a sum of single-particle terms describing the independent motion of each electron in a central potential $V(r)$:

$$H_{\rm CP} = \sum_{i=1}^N \left[\frac{{p_i}^2}{2m} + V(r_i)\right]\,. \quad (24.23)$$

The potential $V(r)$ must describe the nuclear attraction and the electron-electron repulsion as well as possible and must satisfy the boundary conditions

$$V(r)\underset{r\to 0}{\longrightarrow} -Z/r \quad \text{and} \quad V(r)\underset{r\to\infty}{\longrightarrow} -1/r \quad (24.24)$$

in the case of a neutral atom. $H_{\rm CP}$ is separable in spherical coordinates and its eigenstates can be written as Slater determinants of one-electron orbitals of the form $r^{-1}P_{n\ell}Y_{\ell m}(\Omega)$ for bound orbitals and of the form $r^{-1}P_{\varepsilon\ell}(r)Y_{\ell m}(\Omega)$ for continuum orbitals. The one-electron radial wave functions satisfy

$$\frac{d^2P_{\varepsilon\ell}(r)}{dr^2} + 2\left[\varepsilon - V(r) - \frac{\ell(\ell+1)}{2r^2}\right]P_{\varepsilon\ell}(r) = 0\,, \quad (24.25)$$

subject to the boundary condition $P_{\varepsilon\ell}(0) = 0$, and similarly for the discrete orbitals $P_{n\ell}(r)$. Hermann and Skillman [13] have tabulated a widely used central potential for each element in the periodic table as well as radial wave functions for each occupied orbital in the ground state of each element.

24.3.2 High Energy Behavior

The hydrogen atom cross section, which is nonzero at threshold and decreases monotonically with increasing photon energy, serves as a model for inner-shell photoionization cross sections in the x-ray photon energy range. A sharp onset at threshold followed by a monotonic decrease above threshold is precisely the behavior seen in x-ray photoabsorption measurements. A simple hydrogenic approximation at high energies may be justified theoretically as follows: (1) Since a free electron cannot absorb a photon (because of kinematical considerations), at high photon energies one expects the more strongly bound inner electrons to be preferentially ionized as compared with the outer electrons. (2) Since the $P_{n\ell}(r)$ for an inner electron is concentrated in a very small range of r, one expects the integrand of the radial dipole matrix element to be negligible except for those values of r where $P_{n\ell}(r)$ is greatest. (3) Thus it is only necessary to approximate the atomic potential locally, e.g., by means of a screened Coulomb potential

$$V_{n\ell}(r) = -\left(\frac{Z - s_{n\ell}}{r}\right) + V^{\rm o}_{n\ell} \quad (24.26)$$

appropriate for the $n\ell$ orbital. Here $s_{n\ell}$ is the "inner-screening" parameter, which accounts for the screening of the nuclear charge by the other atomic electrons, and $V^{\rm o}_{n\ell}$ is the "outer-screening" parameter, which accounts for the lowering of the $n\ell$ electrons' binding energy due to repulsion between the outer electrons and the photoelectron as the latter leaves the atom. The potential in (24.26) predicts hydrogen-like photoionization cross sections for inner-shell electrons with onsets determined by the outer-screening parameters $V^{\rm o}_{n\ell}$.

Use of more accurate atomic central potentials in place of the screened hydrogenic potential in (24.26) generally enables one to obtain photoionization cross sections in the keV photon energy region to within 10% of the experimental results [14]. For high but still nonrelativistic photon energies, i.e., $\omega \ll mc^2$, the energy dependence of the cross section for the $n\ell$ subshell is [15]

$$\sigma_{n\ell} \sim \omega^{-\ell-\frac{7}{2}}\,. \quad (24.27)$$

24.3.3 Near Threshold Behavior

For photons in the vuv energy region, i.e., near the outer-subshell ionization thresholds, the photoionization cross sections for subshells with $\ell \geq 1$ frequently have distinctly nonhydrogenic behavior. The cross section, instead of decreasing monotonically as for hydrogen, rises above threshold to a maximum (the so called *delayed maximum* above threshold). Then it decreases to a minimum (the *Cooper minimum* [16, 17]) and rises to a second maximum. Finally the cross section decreases monotonically at high energies in acordance with hydrogenic behavior. Such nonhydrogenic behavior may be interpreted as due either to an effective potential barrier or to a zero in the radial dipole matrix element. We examine each of these effects in turn.

The *delayed maximum* above outer subshell ionization thresholds of heavy atoms (i.e., $Z \gtrsim 18$) is due to an effective potential barrier seen by $\ell = 2$ and $\ell = 3$ photoelectrons in the region of the outer edge of the atom [*cf.* Eq. (24.25)]. This effective potential lowers the probability of photoelectron escape until the photoelectrons have enough excess energy to surmount the barrier. Such behavior is nonhydrogenic. Furthermore, in cases where an inner subshell with $\ell = 2$ or 3 is being filled as Z increases (as in the transition metals, the lanthanides and the actinides) there is a double well potential. This double well has profound effects on the $3p$-subshell spectra of the transition metals, the $4d$-subshell spectra of the lanthanides, and the $5d$-subshell spectra of the actinides, as well as on atoms with Z just below those of these series of elements [18, 19].

Cross section minima arise due to a change in sign of the radial dipole transition matrix element in a particular channel [20, 21]. Rules for predicting their occurrence were developed by Cooper [16, 17]. Studies of their occurrence in photoionization from excited states [22], in high Z atoms [23], and in relativistic approximation [24] have been carried out. Only recently has a proof been given [25] that such minima do not occur in atomic hydrogen spectra. For other elements, there are further rules on when and how many minima may occur [26].

Often within such minima, one can observe effects of weak interactions that are otherwise obscured. Relativistic and weak correlation effects on the asymmetry parameter β for s-subshells is a notable example [27]. Wang et al. [28] have also emphasized that near such minima in the E1 amplitudes, one cannot ignore the effects of quadrupole and higher corrections to the differ-

ential cross section. Central potential model calculations [28] show that quadrupole corrections can be as large as 10% of the E1 cross section at such cross section minima, even for low photon energies.

24.4 PARTICLE-HOLE INTERACTION EFFECTS

The experimental photoionization cross sections for the outer subshells of the noble gases[3] near the ionization thresholds can be understood in terms of interactions between the photoelectron, the residual ion, and the photon field which are called, in many-body theory language, "particle-hole" interactions (see Chap. 23). These may be described as interactions in which two electrons either excite or de-excite each other out of or into their initial subshell locations in the unexcited atom. To analyze the effects of these interactions on the cross section, it is convenient to classify them into three categories: intrachannel, virtual double excitation, and interchannel. These alternative kinds of particle-hole interactions are illustrated in Fig. 24.1 using both many-body perturbation theory (MBPT) diagrams and more "physical" scattering pictures. We discuss each of these types of interaction in turn.

24.4.1 Intrachannel Interactions

The MBPT diagram for this interaction is shown on the left in Fig. 24.1(a); on the right a slightly more pictorial description of this interaction is shown. The wiggly line indicates a photon, which is absorbed by the atom in such a way that an electron is excited out of the $n\ell$ subshell. During the escape of this excited electron, it collides or interacts with another electron from the same subshell in such a way that the second electron absorbs all the energy imparted to the atom by the photon; the first electron is de-excited back to its original location in the $n\ell$ subshell. For closed-shell atoms, the photoionization process leads to a $^1P_1$ final state in which the intrachannel interaction is strongly repulsive. This interaction tends to broaden cross section maxima and push them to higher photon energies as compared with the results of central potential model calculations.

Intrachannel interaction effects are taken into account automatically when the correct Hartree-Fock (HF) basis set is employed in which the photoelectron sees a net Coulomb field due to the residual ion and is coupled to the ion to form the appropriate total orbital L and spin

[3]The noble gases have played a prominent role in the development of the theory of photoionization for two reasons. These were among the first elements studied by experimentalists with synchrotron radiation beginning in the 1960's. Also, their closed-shell, spherically symmetric ground states simplified the theoretical analysis of their cross sections.

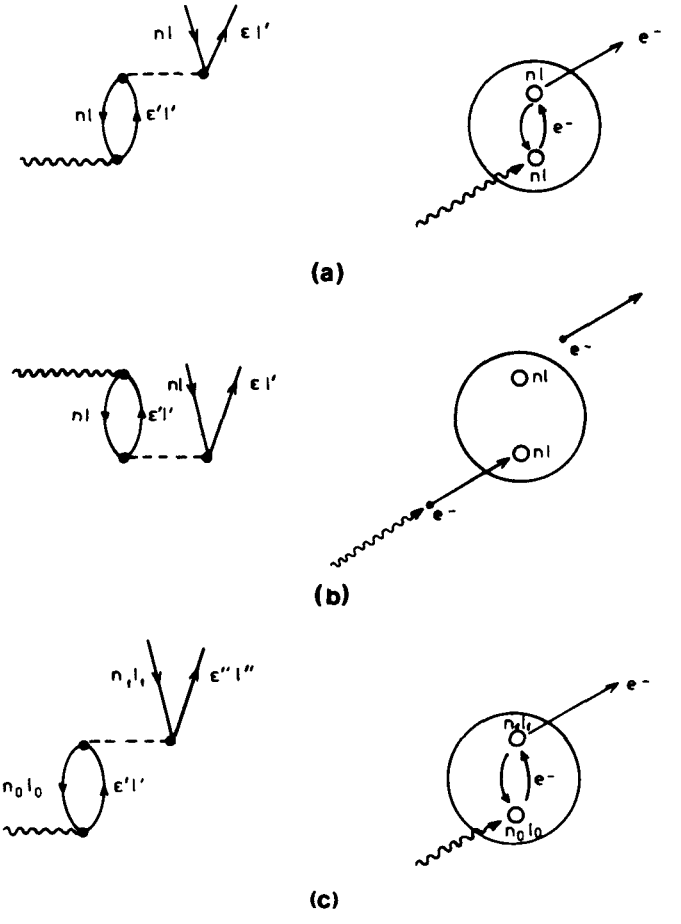

Figure 24.1. MBPT diagrams (left) and scattering pictures (right) for three kinds of particle-hole interaction: (a) intrachannel scattering following photoabsorption; (b) photoabsorption by a virtual doubly-excited state; (c) interchannel scattering following photoabsorption.

S angular momenta. Any other basis set requires explicit treatment of intrachannel interactions.

24.4.2 Virtual Double Excitations

The MBPT diagram for this type of interaction is shown on the left in Fig. 24.1(b). Topologically, this diagram is the same as that on the left in Fig. 24.1(a). In fact, the radial parts of the two matrix elements are identical; only the angular factors differ. A more pictorial description of this interaction is shown on the right of Fig. 24.1(b). The ground state of the atom before photoabsorption is shown to have two electrons virtually excited out of the $n\ell$ subshell. In absorbing the photon, one of these electrons is de-excited to its original location in the $n\ell$ subshell, while the other electron in

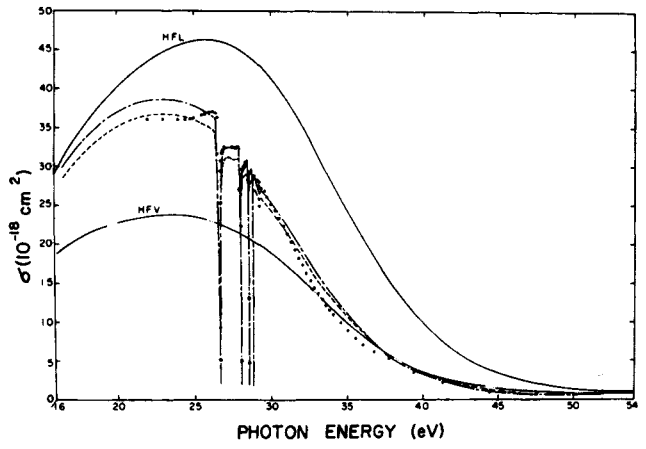

Figure 24.2. Photoionization cross section for the $3p$ and $3s$ subshells of Ar. HFL and HFV indicate the length and velocity results obtained using HF orbitals calculated in a $^1P_1$ potential. Dot-dash and dashed lines represent the length and velocity results of the MBPT calculation of Kelly and Simons [29]. Only the four lowest $3s \rightarrow np$ resonances are shown; the series converges to the $3s$ threshold at 29.24 eV. Experimental results are those of Samson[30] above 37 eV and of Madden *et al.* [31] below 37 eV (From Ref. [29]).

ionized. These virtual double excitations imply a more diffuse atom than in central-potential or HF models, with the effect that the overly repulsive intrachannel interactions are weakened, leading to cross sections for noble gas atoms that are in very good agreement with experiment with the exception that resonance features are not predicted.

24.4.3 Interchannel Interactions

The interchannel interaction shown in Fig. 24.1(c) is important, particularly for s subshells. This interaction has the same form as the intrachannel interaction shown in Fig. 24.1(a), except now when an electron is photoexcited out of the $n_0\ell_0$ subshell, it collides or interacts with an electron in a different subshell—the $n_1\ell_1$ subshell. This interaction causes the second electron to be ionized, and the first electron to fall back into its original location in the $n_0\ell_0$ subshell.

Interchannel interaction effects are usually very conspicuous features of photoionization cross sections. When the interacting channels have partial photoionization cross sections which differ greatly in magnitude, one finds that the calculated cross section for the weaker channel is completely dominated by its interaction with the stronger channel. At the same time, it is often a safe approximation to ignore the effect of weak channels on stronger channels. In addition, when the interacting channels have differing binding energies, their interchannel interactions lead to resonance structure in the channel with lower binding energy (arising from its coupling to the Rydberg series in the channel with higher binding energy).

24.4.4 Photoionization of Ar

An example of both the qualitative features exhibited by photoionization cross sections in the vuv energy region and of the ability of theory to calculate photoionization cross reactions is provided by photoionization of the $n = 3$ subshell of argon, i.e.,

$$\begin{aligned} \mathrm{Ar}3s^2 3p^6 + \gamma &\rightarrow \mathrm{Ar}^+ 3s^2 3p^5 + \mathrm{e}^- \\ &\rightarrow \mathrm{Ar}^+ 3s 3p^6 + \mathrm{e}^- . \end{aligned} \tag{24.28}$$

Figure 24.2 shows the MBPT calculation of Kelly and Simons [29], which includes both intrachannel and interchannel interactions as well as the effect of virtual double excitations. The cross section is in excellent agreement with experiment [30, 31], even to the extent of describing the resonance behavior due to discrete members of the $3s \rightarrow \varepsilon p$ channel.

Figure 24.2 illustrates most of the features of photoionization cross sections described so far. First, the cross section rises to a delayed maximum just above the threshold because of the potential barrier seen by photoelectrons from the $3p$ subshell having $\ell = 2$. For photon energies in the range of 45 eV–50 eV, the calculated cross section goes through a minimum because of a change in sign of the $3p \rightarrow \varepsilon d$ radial dipole amplitude. The HFL and HFV calculations include the strongly repulsive intrachannel interactions in the ^1P final-state channels and calculate the transition amplitude using the length (L) and velocity (V) form respectively for the electric dipole transition operator [*cf.* Eq. (24.7)]. With respect to the results of central potential model calculations, the HFL and HFV results have lower and broader maxima at higher energies. They also disagree with each other by a factor of two! Inclusion of virtual double excitations results in length and velocity results that agree to within 10% with each other and with experiment, except that the resonance structures are not reproduced. Finally, taking into account the interchannel interactions, one obtains the length and velocity form results shown in Fig. 24.2 by dash-dot and dashed curves respectively. Agreement with experiment is excellent and the observed resonances are well-reproduced.

24.5 THEORETICAL METHODS FOR PHOTOIONIZATION

24.5.1 Calculational Methods

Most of the *ab initio* methods for the calculation of photoionization cross sections (e.g., the MBPT method [32], the close-coupling (CC) method [33], the R-matrix method [34], the random phase approximation (RPA) method [8], the relativistic RPA method [35], the transition matrix method [36], the multiconfiguration Hartree-Fock (MCHF) method [37,38], etc.) have successfully calculated outer p-subshell photoionization cross sections of the noble gases by treating in their alternative ways the key interactions described above, i.e., the particle-hole interactions. In general, these methods all treat both intrachannel and interchannel interactions to infinite order and differ only in their treatment of ground state correlations. (The exception is MBPT, which often treats interchannel interactions between weak and strong channels only to first or second order.) These methods therefore stand in contrast to central potential model calculations, which do not treat any of the particle-hole interactions, and single-channel term-dependent HF calculations, which treat only the intrachannel interactions. The key point is that selection of the interactions that are included in a particular calculation is more important than the method by which such interactions are handled.

Treatment of photoionization of atoms other than the noble gases presents additional challenges for theory. For example, elements such as the alkaline earths, which have s^2 outer subshells, require careful treatment of electron pair excitations in both initial and final states. Open shell atoms have many more ionization thresholds than do the noble gases. Treatment of the resultant rich resonance structures typically relies heavily on quantum defect theory [38] (see Chap. 45). All the methods listed above can be used to treat elements other than the noble gases, but a method which has come to prominence because of the excellent results it obtains for both alkaline earth and open-shell atoms is the eigenchannel R-matrix method [39].

24.5.2 Other Interaction Effects

A number of interactions, not of the particle-hole type, lead to conspicuous effects in localized energy regions. When treating photoionization in such energy regions, one must be careful to choose a theoretical method which is appropriate. Among the interactions which may be important are the following:

Relativistic and Spin-Dependent Interactions. The fact that $j = \ell - \frac{1}{2}$ electrons are contracted more than $j = \ell + \frac{1}{2}$ electrons at small distances has an enormous effect on the location of cross section minima in heavy elements [14,40]. It may explain the large observed differences in the profiles of a resonance decaying to final states that differ only in their fine structure quantum numbers [41].

Inner-Shell Vacancy Rearrangement. Inner-shell vacancies often result in significant production of satellite structures in photoelectron spectra. Calculations for inner subshell partial photoionization cross sections are often substantially larger than results of photoelectron measurements [42–44]. This difference is attributed to such satellite production, which is often not treated in theoretical calculations.

Polarization and Relaxation Effects. Negative ion photodetachment cross sections often exhibit strong effects of core polarization near threshold. These effects can be treated semi-empirically, resulting in excellent agreement between theory and experiment [45]. Even for inner shell photoionization cross sections of heavy elements, *ab initio* theories do not reproduce measurements near threshold without the inclusion of polarization and relaxation effects [46,47].

An Example. The calculation of the energy dependence of the asymmetry parameter β for the $5s$ subshell of xenon requires the theoretical treatment of all of the above effects. In the absence of relativistic interactions, β for Xe$5s$ would have the energy-independent value of two. Deviations of β from two are therefore an indication of the presence of these relativistic interactions. The greatest deviation of β from two occurs in the localized energy region where the partial photoionization cross section for the $5s$ subshell has a minimum. In this region, however, relativistic calculations show larger deviations from two than are observed experimentally. Inner shell rearrangement and relaxation effects play an important role [48,49] and must be included to achieve good agreement with experiment.

24.6 FUTURE DIRECTIONS

The construction of high brightness synchrotron light sources and the increasing use of lasers are providing the means to study atomic photoionization processes at an unparalleled level of detail. The synchrotrons generally produce photons in the soft x-ray and x-ray regions. Thus, inner shell vacancy production and decay, satellite production, and multiple ionization phenomena are all being increasingly studied. Laser sources are allowing production of atoms in tailored initial states. Thus, photoionization of excited atoms and, in particular, complete measurements of particular photoionization processes, are now possible. Recent collections of short review papers provide references to these topics [3,4]. In addition, two recent reviews of experimental results for noble gas atom photoionization [50] and for metal atom

photoionization [51] provide also valuable information on the current state of the corresponding theoretical results.

REFERENCES

1. A. F. Starace, in *Handbuch der Physik*, edited by W. Mehlhorn (Springer, Berlin, 1982), Vol XXXI, pp. 1–121.
2. M. Ya. Amusia, *Atomic Photoeffect* (Plenum, New York, 1990).
3. *Many-Body Theory of Atomic Structure and Photoionization*, edited by T. N. Chang (World Scientific, Singapore, 1993).
4. *VUV and Soft X-Ray Photoionization Studies*, edited by U. Becker and D. A. Shirley (in press) (Plenum, New York, 1996).
5. J. J. Sakurai, *Advanced Quantum Mechanics* (Addison-Wesley, Reading, 1967), p. 39.
6. S. Chandrasekhar, Astrophys. J. **102**, 223 (1945).
7. A. F. Starace, Phys. Rev. A **3**, 1242 (1971); **8**, 1141 (1973).
8. M. Ya. Amusia and N. A. Cherepkov, Case Studies in At. Phys. **5**, 47 (1975).
9. J. M. Blatt and L. C. Biedenharn, Rev. Mod. Phys. **24**, 258 (1952).
10. *cf.* Sect. 7 of Ref. [1].
11. C. N. Yang, Phys. Rev. **74**, 764 (1948).
12. See, e.g., Eqs. (9.6)–(9.15) of [1] for expressions for the reduced matrix elements in Eq. (24.22) in which all angular integrations have been carried out and the results are expressed in terms of one-electron radial dipole matrix elements.
13. F. Hermann and S. Skillman, *Atomic Structure Calculations* (Prentice-Hall, Englewood Cliffs, 1963).
14. R. H. Pratt, A. Ron, and H. K. Tseng, Rev. Mod. Phys. **45**, 273 (1973).
15. H. A. Bethe and E. E. Salpeter, *Quantum Mechanics of One- and Two-Electron Atoms* (Springer, Berlin, 1957), Sects. 69–71.
16. J. W. Cooper, Phys. Rev. **128**, 681 (1962).
17. U. Fano and J. W. Cooper, Rev. Mod. Phys. **40**, 441 (1968).
18. Ref. [1], pp. 50–55, and references therein.
19. *Giant Resonances in Atoms, Molecules, and Solids*, edited by J. P. Connerade, J. M. Estiva, and R. C. Karnatak (Plenum, New York, 1987), and references therein.
20. D. R. Bates, Mon. Not. R. Astron. Soc. **106**, 432 (1946).
21. M. J. Seaton, Proc. Roy. Soc. A **208**, 418 (1951).
22. A. Z. Msezane and S. T. Manson, Phys. Rev. Lett. **48**, 473 (1982).
23. Y. S. Kim, R. H. Pratt, and A. Ron, Phys. Rev. A **24**, 1626 (1981).
24. Y. S. Kim, A. Ron, R. H. Pratt, B. R. Tambe, and S. T. Manson, Phys. Rev. Lett. **46**, 1326 (1981).
25. S. D. Oh and R. H. Pratt, Phys. Rev. A **34**, 2486 (1986).
26. R. H. Pratt, R. Y. Yin, and X. Liang, Phys. Rev. A **35**, 1450 (1987); R. Y. Yin and R. H. Pratt, Phys. Rev. A **35**, 1149 (1987); **35**, 1154 (1987).
27. S. T. Manson and A. F. Starace, Rev. Mod. Phys. **54**, 389 (1982).
28. M. S. Wang, Y. S. Kim, R. H. Pratt, and A. Ron, Phys. Rev. A **25**, 857 (1982).
29. H. P. Kelly and R. L. Simons, Phys. Rev. Lett. **30**, 529 (1973).
30. J. A. R. Samson, Adv. At. Mol. Phys. **2**, 177 (1966).
31. R. P. Madden, D. L. Ederer, and K. Codling, Phys. Rev. **177**, 136 (1969).
32. H. P. Kelly in *Photoionization and Other Probes of Many-Electron Interactions*, edited by F. J. Wuilleumier (Plenum, New York, 1976), pp. 83–109.
33. P. G. Burke and M. J. Seaton, Methods Comput. Phys. **10**, 1 (1971).
34. P. G. Burke and W. D. Robb, Adv. At. Mol. Phys. **11**, 143 (1975); *Electronic and Atomic Collisions: Invited Papers and Progress Reports*, edited by G. Watel (North Holland, Amsterdam, 1978), pp. 201–280.
35. W. R. Johnson, C. D. Lin, K. T. Cheng, and C. M. Lee, Phys. Scr. **21**, 409 (1980).
36. T. N. Chang and U. Fano, Phys. Rev. A **13**, 263 (1976); **13**, 282 (1976).
37. J. R. Swanson and L. Armstrong, Jr., Phys. Rev. A **15**, 661 (1977); **16**, 1117 (1977).
38. M. J. Seaton, Rep. Prog. Phys. **46**, 167 (1983).
39. C. H. Greene, in *Fundamental Processes of Atomic Dynamics*, edited by J. S. Briggs, H. Kleinpoppen, and H. O. Lutz (Plenum, New York, 1988), pp. 105–127, and references therein.
40. D. W. Lindle, T. A. Ferrett, P. A. Heiman, and D. A. Shirley, Phys. Rev. A **37**, 3808 (1988).
41. M. Krause, F. Cerrina, A. Fahlman, and T. A. Carlson, Phys. Rev. Lett. **51**, 2093 (1983).
42. J. B. West, P. R. Woodruff, K. Codling, and R. G. Houlgate, J. Phys. B **9**, 407 (1976).
43. M. Y. Adam, F. Wuilleumier, N. Sandner, V. Schmidt, and G. Wendin, J. Phys. (Paris) **39**, 129 (1978).
44. U. Becker, T. Prescher, E. Schmidt, B. Sonntag, and H.-E. Wetzel, Phys. Rev. A **33**, 3891 (1986).
45. See, e.g., K. T. Taylor, and D. W. Norcross, Phys. Rev. A **34**, 3878 (1986).
46. M. Ya. Amusia, in *Atomic Physics 5*, edited by R. Marrus, M. Prior, and H. Shugart (Plenum, New York, 1977), pp. 537–565.
47. W. Jitschin, U. Werner, G. Materlik, and G. D. Doolen, Phys. Rev. A **35**, 5038 (1987).
48. G. Wendin and A. F. Starace, Phys. Rev. A **28**, 3143 (1983).
49. J. Tulkki, Phys. Rev. Lett. **62**, 2817 (1989).
50. V. Schmidt, Rep. Prog. Phys. **55**, 1483 (1992).
51. B. Sonntag and P. Zimmerman, Rep. Prog. Phys. **55**, 911 (1992).